Composites: Part A 139 (2020) 106120

Contents lists available at ScienceDirect

Composites Part A

journal homepage: www.elsevier.com/locate/compositesa

Investigation of the interphase mechanisms and welding behaviour of fast-curing epoxy based composites with co-cured thermoplastic boundary layers

Lucian Zweifel *, Christian Brauner

Institute of Polymer Engineering, FHNW University of Applied Sciences and Arts, Switzerland

ARTICLE INFO

Keywords:
Thermosetting resin (A)
Interphase (B)
Mechanical testing (D)
Joining (E)

ABSTRACT

This study focuses on investigating thermoplastic polymers and their interphase behaviour with the fast-curing epoxy system Araldite LY3585/Aradur 3475. The three compatible thermoplastic polymers poly(methyl methacrylate) (PMMA), amorphous polyamide (PA12TR90), and poly(hydroxy ether) (phenoxy) were chosen to determine their affinity and interphase formation with the epoxy system. The final concept involves the use of a thermoplastic as a boundary layer on top of the epoxy to establish a connection between two joined parts by resistance welding. The thermoplastic boundary layer was generated by co-curing during the curing process. The experiments resulted in a high compatibility between phenoxy and PMMA in the selected epoxy system which leads to excellent mechanical properties after welding. Phenoxy showed the strongest joints, with an average lap shear strength of 25 MPa, demonstrating the high potential of this joining technique for industrial applications in the automotive and wind energy fields.

1. Introduction

The combination of materials has been fully integrated into today's industry to simultaneously apply the specific advantages of certain materials to specific applications. In the aerospace and automotive fields, fibre-reinforced materials are becoming increasingly common to replace heavy materials such as steel and aluminium in order to reduce vehicle weight and thus CO_2 emissions significantly [1]. Fibre-reinforced composites contribute to the environmental challenge of sustainable mobility. The efficient joining of fibre-reinforced thermoset materials for industrial applications is key to enabling lightweight design concepts with the premise of applying the right material in the right place. One possible application of this approach is the use of thermoplastic boundary layers, which make it possible to weld thermoset components [2–4] in fibre-reinforced composite components. Thermoplastic welding methods have certain advantages over traditional joining techniques such as very short process times (<5 min) and strong, reliable joints without significant surface preparation efforts (cleaning, grinding, inspection, etc.). Traditional technologies such as bolted joints and adhesive bonding are not the most suitable for fibre-reinforced composite structures [5]. The problem with adhesive bonding lies mainly in the time-consuming surface pre-treatment required to achieve sufficient adhesion, which results in high costs. Riveted or bolted joints lead to high stress concentrations around the drilled holes and thus heavier or costlier designs. Thus, there is a need for an efficient joining technique which can afford strong, cost-effective, and reliable joints. Thermoplastic welding, with the capability for melting and reprocessing, offers advantages over thermosets, which cannot be re-melted once they are cured [1].

An attractive approach to using the thermoplastic welding process for thermosets is to co-cure a thermoplastic boundary layer during the curing of a thermoset resin. This leads to a weldable surface which can be processed with thermoplastic welding methods such as resistance welding [6,7], ultrasonic welding [4,8], or induction welding. Upon co-curing the thermoplastic boundary layer onto an epoxy system, the thermoset precursors partially dissolve and then diffuse into the thermoplastic, followed by reaction-induced phase separation. Simultaneously, the dissolved thermoplastic monomers become mobile and begin to diffuse into the thermoset. The diffusion rate depends on the local concentration, the affinities of the components of the epoxy resin and thermoplastic polymer, and their respective molecules [4]. One favourable mechanism is a gradient interphase where the overall cross-link density of the material varies from location to location on the macroscopic level. This involves partial swelling of the thermoplastic

* Corresponding author at: Klosterzelgstrasse 2, 5210 Windisch, Switzerland.
E-mail address: lucian.zweifel@fhnw.ch (L. Zweifel).

https://doi.org/10.1016/j.compositesa.2020.106120
Received 9 July 2020; Received in revised form 29 August 2020; Accepted 15 September 2020
Available online 23 September 2020

film followed by fast polymerisation of the thermoset before diffusional equilibrium takes place [9]. As curing continues, the molecular weight increases, inducing a shift in the decomposition temperature. The critical composition line eventually passes the curing temperature and triggers a phase separation [3,10]. This process is dependent on the pressure, temperature, and concentration of the two phases [11]. The result is a pronounced heterogeneous morphology with a thermoplastic-rich phase and a thermoset-rich phase and strong mechanical interlocking at the micrometre scale [7]. Suitable material combinations for the high-temperature ranges used in aerospace related applications have been well researched [6,7,10,12]. Polyetherimide (PEI), an amorphous thermoplastic, is an ideal selection for toughening and co-curing. Thus, high average lap shear strengths above 35 MPa were achieved with minimal process times by performing resistance [2,7] or ultrasonic [4,13] welding. This is strong evidence of the potential of this joining technology. For aerospace applications, a comparable adhesive is FM® 309–1 (Solvay) for bonding composite and metallic structures resulting in a lap shear strength of 42 MPa with process conditions of 180 °C for 3 h [14]. For automotive applications, a comparable structural adhesive is SikaPower® 1200 with a lap shear strength of 20 MPa and processing time of 2 h at 90 °C [15].

The present paper aims at assessing whether it is feasible to create a pronounced interphase between thermoplastic materials and a thermoset polymer with a fast curing cycle (less than 10 min) that is typically used for automotive applications. The glass transition temperature of the selected epoxy system is approximately 120 °C and therefore meets the requirements of transportation areas such as the automotive and railway sectors, as well as wind energy. There is significant potential for improving the process by introducing a thermoplastic boundary layer to be used for welding or the integration of functional components by injection moulding in a so-called over moulding step. In this study, a review of possible polymer candidates was performed, and three thermoplastic polymers were tested in detail to create a coupling zone with a stronger interlocking mechanism than usual adhesion forces (e.g. glued joints) [16]. First, optical hot-stage experiments were performed to investigate the affinity of the three thermoplastic films towards the epoxy resin. Next, an innovative manufacturing process was derived based on a modified vacuum infusion (MVI) setup coupled with co-curing of the thermoplastic boundary layer to produce composite plates, the interphases of which were analysed by preparing cross-section samples. Furthermore, Raman spectroscopy was used to quantify the size of the interphase and compare optical analysis methods. Finally, the composite plates were used to develop a reliable resistance welding process. With the optimised parameters, an average lap shear strength based on ASTM D1002 of 25 MPa was achieved for the poly (hydroxy ether) (phenoxy)/glass-fibre-reinforced polymer (GFRP) system.

2. Experimental

2.1. Materials

2.1.1. Thermoset material

In this study, an epoxy resin system (Araldite LY3585/Aradur 3475) provided by Huntsman Advanced Materials (Basel, Switzerland) was used. The system is widely applied in the mass production of automotive components and is notable for its short curing cycles and final glass transition temperature of approximately 120 °C. The mentioned system is made for high-pressure resin transfer moulding (RTM) and wet compression moulding applications with a curing cycle of 2 min at 115 °C respectively 1 min at 140 °C. High pressure RTM coupled with a similar type of epoxy resin system is used for series-production of the BMW i3 passenger cell [17]. It is based on bisphenol-A-diglycidylether as a resin and 1,3-cyclohexanedimethanamine and methyldiethanolamine as hardeners. A kinetic model was developed using the modified Kamal–Sourour model according to Garsche et al. [18] to describe the curing process. The model is essential for monitoring the previously mentioned physico-chemical events which take place during optical hot-stage microscopy and depend on temperature and time. The Kamal–Sourour model does not consider diffusion-controlled reactions [18]. Thus, chemically controlled reactions are modelled well, but after reaching the glass transition line, curing is mainly influenced by diffusion. Therefore, modified models have been introduced with an empirical diffusion term to describe both chemically and diffusion-controlled curing. The chosen amine-cured epoxy resin model takes into consideration diffusion-controlled cross-linking in the final stage of the curing reaction by adding a semi-empirical term based on free volume theory [18]:

$$f_d = \frac{1}{1 + \exp(C_1(\alpha - \alpha_c))}. \tag{1}$$

Here, f_d is the diffusion factor, α is the degree of cure, α_c is the critical degree of cure and a linear function of temperature and C_1 is a design parameter. The maximum achievable α_c, which is defined as the end of the reaction, was calculated by fitting experimental isothermal curing data with expression (2) in order to understand the curing behaviour at various temperatures and times

$$\alpha_c = \min f_0(1, C_2 + TC_3), \tag{2}$$

where T is the temperature, C_2 and C_3 are design parameters. This provides a representation of both the end of the reaction and the early deceleration of curing when the system reaches the glass transition temperature, which is above its curing temperature. The full form of the equation is

$$\frac{\partial \alpha}{\partial t} = \frac{\left[A_1 exp\left(-\frac{E_1}{RT}\right) + A_2 exp\left(-\frac{E_2}{RT}\right)\alpha^m\right](1-\alpha)^n}{1 + exp[C_1(\alpha - min(1, C_2 + TC_3))]}, \tag{3}$$

in which A_1 and A_2 are Arrhenius terms, E_1 and E_2 are activation energies, and m and n are order of reactions. Differential scanning calorimetry (DSC) measurements were used with a non-linear optimisation strategy to optimise the data to the modified Kamal–Sourour model. Hence, the objective function is defined as a minimization problem to find the smallest difference between experimental data and the model. Table 1 summarises the determined parameters. As a useful visualisation, the kinetic model was applied to isothermal curing conditions to demonstrate their effect on the degree of curing (Fig. 1).

2.1.2. Thermoplastic materials

The key element for forming a gradient interphase is the material combination. Thermoplastic materials were selected based on several criteria such as operating temperature, morphology, solubility, diffusion behaviour, and structural properties. Poly(methyl methacrylate) (PMMA), polyamide (PA12TR90), and phenoxy present amorphous morphologies and favourable glass transition temperatures that potentially allow dissolution and diffusion during co-curing. Additionally, the creep behaviour, strength, and impact resistance must be considered. However, the mechanical properties strongly depend on the application, whereas this study focused on investigating the interphase behaviour.

Table 1
Parameters for the Kamal–Sourour model of the epoxy system.

Curing kinetic parameter	Value
Arrhenius term A_1 (s^{-1})	1379543.2
Activation energy E_1 (J mol^{-1} K^{-1})	58893.3
Arrhenius term A_2 (s^{-1})	57665.4
Activation energy E_2 (J mol^{-1} K^{-1})	45949.5
Reaction order m (-)	1.85
Reaction order n (-)	1.71
Constant C_1 (-)	131.6
Constant C_2 (-)	−0.037202
Constant C_3 (K^{-1})	0.002568

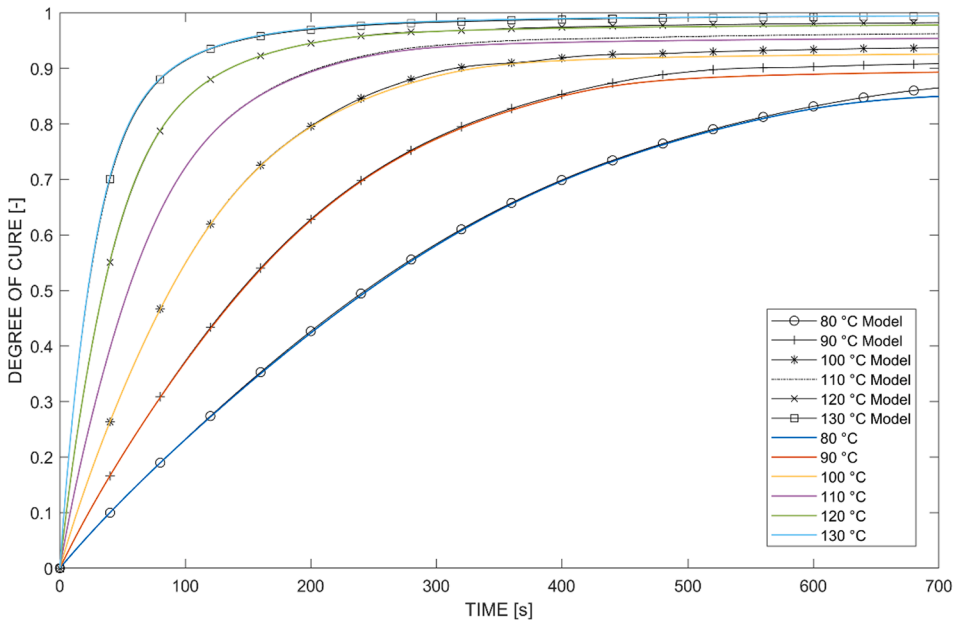

Fig. 1. Comparison of isothermal DSC measurements with the curing kinetic model of the epoxy system of Araldite LY3585/Aradur 3475. (For interpretation of the references to colour in this figure legend, the reader is referred to the web version of this article.)

Thus, Table 2 presents an overview of the three selected thermoplastic materials which exhibit favourable thermal and transport properties. [19–21]

2.2. Optical hot-stage microscopy

An optical hot-stage microscopy setup was used according to Teuwen et al. [3] where a controlled heating device (Linkam) was coupled with optical microscopy (Keyence VHX 600) to investigate the microstructural behaviour as a function of temperature (Fig. 2). The thermoplastic films were cut to 10 × 25 mm^2 and a thickness of 125 µm. First, each thermoplastic film was heated at a rate of 50 K min^{-1} to above the glass transition temperature (PMMA: 150 °C, PA12TR90: 200 °C, phenoxy: 110 °C) to bond the cover glass and film together. A toothpick was used to press the thermoplastic and cover glass together to ensure a good connection. Then, the temperature was decreased to the curing temperature, which was fixed to 100 °C in this study. As soon as the curing temperature was reached, the epoxy resin (Araldite LY3585) was mixed with the amine hardener (Aradur 3475). After a homogenous mixture was achieved, a toothpick was used to fill the cavity with epoxy resin. A time-lapse program was used to capture an image every 15 s in order to characterise the interphase.

2.3. Manufacturing of composite plates, interphase microscopy and spectroscopy

MVI was chosen as a simplified lab-scaled process that is representative to an industrial process such as high-pressure RTM. The aim was to manufacture glass-fibre-reinforced composite plates towards a detailed study of the interphase as a starting point for welding and mechanical assessments of the lap shear strength properties of the connections. Additionally, it was essential to see if it was possible to seal the thermoplastic boundary layer in a targeted manner that no epoxy resin flows beneath the film. This combination of a liquid resin moulding process in combination with the co-curing process of a thermoplastic film is different from the state of art because many researchers with targeting aerospace applications used prepreg materials with a higher viscosity [2,4,7].

Composite plates were manufactured with eight layers of four-harness satin (4HS) weave glass fibre fabric with an aerial weight of 200 g/m^2. The layup was $[0/90, 0/90, 90/0, 90/0]_s$ with a thermoplastic boundary layer on one side having a thickness of 125 µm. The plate was cured for 7 min at 100 °C. A glass fibre fabric was selected because it allows a clearer visual inspection of the sample after manufacturing, welding and testing. There is a dependency of the lap shear strength on the type of fabric [22]. Hence, a satin weave was chosen to reduce the sensitivity of the fibre orientation.

To manufacture test coupons with the thermoplastic boundary layer, a co-curing process [2] was combined with MVI. The thermoplastic film was attached to the surface with tape to avoid resin flow beneath the boundary layer. Then, an infusion stack including a flow medium, perforated foil, and connections for the infusion was placed on top (Fig. 3).

After curing, microsection and Raman spectroscopy analyses of the composite plate were performed. For each plate, several samples were taken for polishing, micro- and spectroscopy. In these observations, the connection area between the thermoplastic and epoxy is essential. Scanning electron microscopy (SEM) was used to obtain a more detailed view of the intersections formed between the epoxy and thermoplastics. The samples were not etched before the measurements because the solvent was in most cases too aggressive and completely destroyed the interphase area. A confocal Raman microspectrometer (Horiba XploRA™ PLUS) was used to perform line scans that allow an assessment of the thickness and shape of the interphases. The line scans were

Table 2
Selected thermoplastic materials for screening of their interphase formation behaviours [24,26]

Material	Tradename	Morphology	T_g	Molecular weight	Tensile strength	Diffusion behaviour
Polymethylmethacrylate (PMMA) [21]	Röhm No. 99,524	Amorphous	110 °C	110.12 g/mol	70 MPa	++ [26,27]
Polyamide (PA12TR90) [20]	Grilamid TR90	Amorphous	155 °C	438.7 g/mol	60 MPa	N.A.
Poly hydroxy ether (phenoxy) [19]	Gabriel Chemical (PKFE)	Amorphous	80 °C	>1000 g/mol	65 MPa	++ [24]

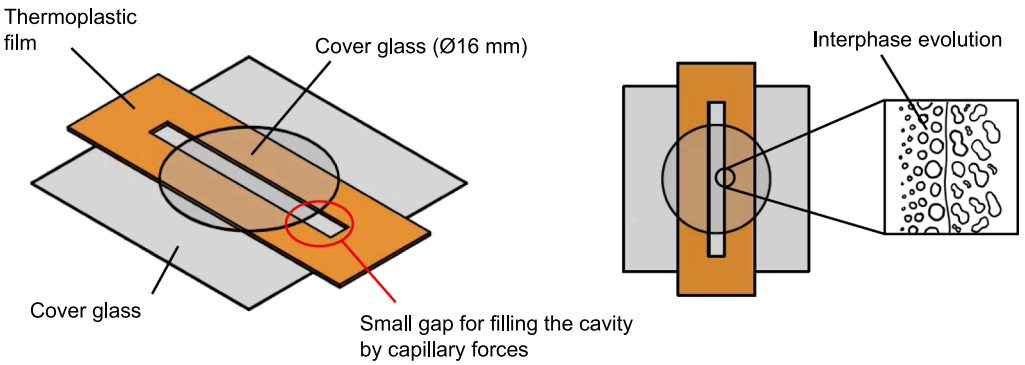

Fig. 2. Measurement stack of the hot-stage microscope with an epoxy gap in a thermoplastic film [3]. (For interpretation of the references to colour in this figure legend, the reader is referred to the web version of this article.)

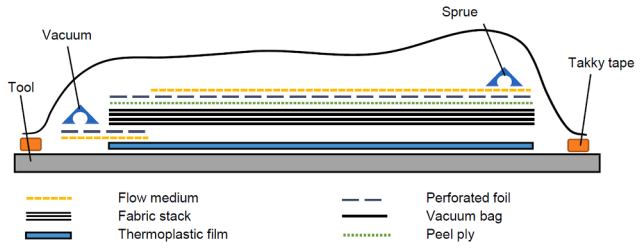

Fig. 3. Schematic for manufacturing hybrid composite plates with the MVI setup. (For interpretation of the references to colour in this figure legend, the reader is referred to the web version of this article.)

performed with 150 spectra over a length of 30 µm, resulting in a step size of 0.2 µm.

2.4. Welding and testing

The custom-built resistance welding setup developed in a previous work [7] was used to determine the welding quality of the samples by single-lap shear tests. First, an experiment was performed with PMMA/GFRP coupons to determine the appropriate nominal process parameters of power [kW/m^2], pressure [MPa], and time [s]. Afterwards, the process parameters were adapted to PA12TR90/GFRP and phenoxy/GFRP. Additionally, the welding behaviour and impregnation of the welding mesh were observed by visually comparing the welded surfaces. A stainless-steel heating element with a wire diameter of 36 µm, a mesh size of 50 µm and an open area of 33.8% was used [23]. The heating elements were cut to dimensions of 12.7 mm wide and 50 mm long.

The welded joints were mechanically tested following the ASTM D1002 standard in a Zwick 100 kN universal tensile test machine with a testing speed of 1.3 mm/min to determine the apparent lap shear strength (LSS). The lap shear strength was calculated as the maximum load divided by the overlap area. Furthermore, fractured specimens were analysed by visual examination of the fracture area [1].

3. Results and discussion

3.1. Interphase formation observed by optical hot-stage microscopy

Fig. 4 presents an image captured at the beginning of curing, exactly when the cavity was filled (left). The last image, shown on the right side, corresponds to the maximum degree of curing and highlights the potential interphase area between the thermoset and thermoplastic materials. It is difficult to observe strongly pronounced formation mechanisms with optical hot-stage microscopy. The fast curing reaction (less than 5 min) limits the interphase evolution in every step. Especially, dissolution and diffusion are less pronounced and depend strongly on time, chain mobility, and curing temperature. Nevertheless, the hot-stage experiments presented an interesting overview of the chosen thermoplastic materials.

PMMA exhibited clear interphase formation (a blend with a concentration gradient) and can be compared to the formation mechanisms observed in PEI/thermoset investigations [3,10,13]. The occurrence of simultaneous diffusion, swelling, and dissolution were verified but were not highly pronounced. The beginning and end of the phase separation were clearly observed in these trials due to the changes in morphology and colour. An estimated interphase thickness of approximately 10–20 µm was reached, which indicates the fast reactivity of the epoxy system.

PA12TR90 presented no affinity towards the epoxy system. This is mainly due to its low chain mobility at 100 °C with respect to the glass transition temperature of the thermoplastic material of approximately 155 °C. In this case, the curing temperature could be increased to the detriment of the reactivity, which is significantly higher at 120 °C. Thus, a compromise must be made to ensure good diffusion and phase separation at a temperature suitable for dissolving the material. Nevertheless, this thermoplastic material does not show satisfactory interphase properties.

Phenoxy exhibited a different interphase formation mechanism. First, dissolution was dominant due to the high affinity of both constituents. Then, simultaneous diffusion occurred in both directions starting from phenoxy into the epoxy system and vice versa. Nevertheless, it was not possible to determine information such as the diffusion rate because the colour and contrast of the materials are almost identical. This solubility behaviour was also observed with RTM6 as an epoxy system, where a phenoxy filament with a diameter of 100 µm was dissolved in 3 min at 140 °C and in 15 min at 120 °C [24]. In this study, no reaction-induced phase separation occurred in the experiments at 100 °C. The critical composition line will eventually cross the curing temperature and trigger a phase separation at different temperatures.

3.2. Interphase micro- and spectroscopy of manufactured composite plates

The thickness of the consolidated plates was approximately 2 mm. The quality was consistent for all the manufactured plates, with a low quantity of pores and a constant fibre volume content of approximately 55% (Fig. 5). An advantage of this coupled process is that no release agent was necessary due to the good demoulding with the thermoplastic boundary layer facing the tool direction. PMMA and phenoxy showed excellent linkage whereas PA12TR90 showed no connection to the GFRP. Therefore, PA12TR90 samples were not used for interphase micro- and spectroscopy.

The SEM images at magnifications of 6.25 and 12.5 kx of PMMA/GFRP presented detailed phase separation (Fig. 6). Two different separation mechanisms were visible, one occurring in the thermoplastic-rich area and the other in the thermoset-rich area. The thickness of the

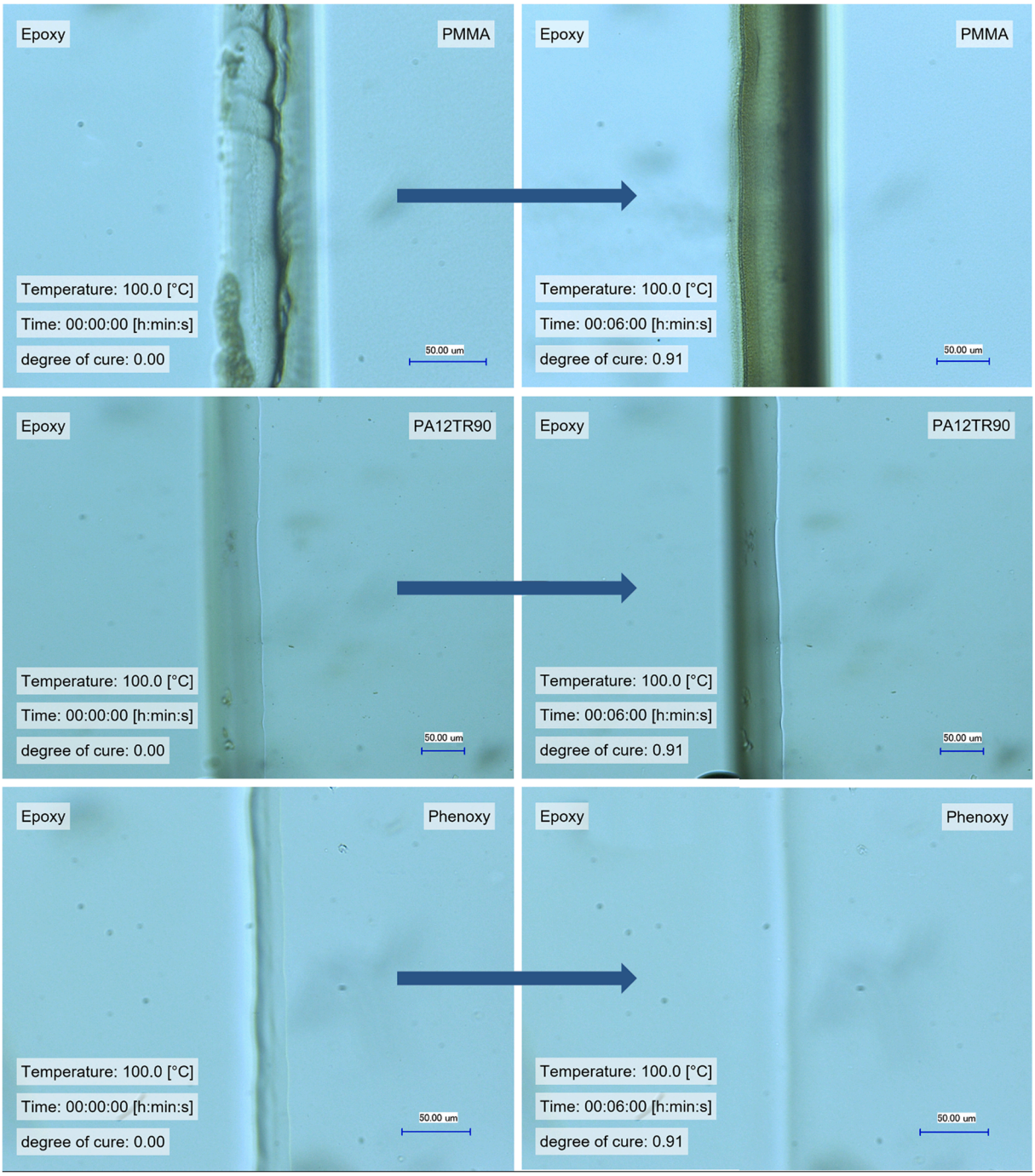

Fig. 4. Optical hot-stage microscopy images of the selected thermoplastics and epoxy system LY3585/3475 at 100 °C. From top to bottom: PMMA, PA12TR90, and phenoxy, where the left image shows a degree of curing of 0 and the right shows the maximum degree of curing. (For interpretation of the references to colour in this figure legend, the reader is referred to the web version of this article.)

gradient interphase was estimated to be 10–20 μm. The phenoxy/GFRP sample (Fig. 7) was imaged at the same magnifications. The boundary edge between the epoxy and thermoplastic was clearer than in the optical hot-stage experiments. This boundary edge presented the same shape as that observed in the hot-stage experiments, where the phenoxy is continuously dissolved by the epoxy system until a diffusional equilibrium is reached due to the reactivity. Especially, in the region below the pure thermoplastic material, there must be a concentration change from phenoxy to the epoxy. Nonetheless, this should be investigated in more detail by Raman spectroscopy.

Raman measurements were performed to quantify the thickness and shape of the interphases in the PMMA/GFRP and phenoxy/GFRP samples. Table 3 shows the experimentally determined parameters for both material combinations. The main challenge of this experiment was the fluorescence of all the used materials. However, the ideal spectral responses were achieved by photobleaching [17] and the use of laser wavelengths of 532 and 638 nm. Fig. 8 shows the single spectra of PMMA, phenoxy, and the cured epoxy system, where the signals were corrected with satisfactory baseline fitting. The difficulty with distinguishing phenoxy and epoxy is readily apparent to the naked eye. Both phenoxy and the epoxy system are based on bisphenol A, which results in similar Raman spectra (Fig. 8). Nevertheless, line scans were

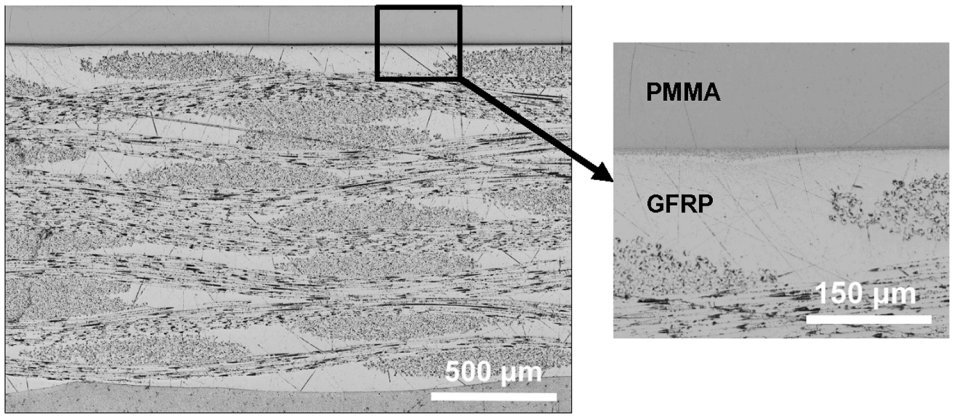

Fig. 5. Cross-sectional optical micrographs of the PMMA/GFRP plate sample.

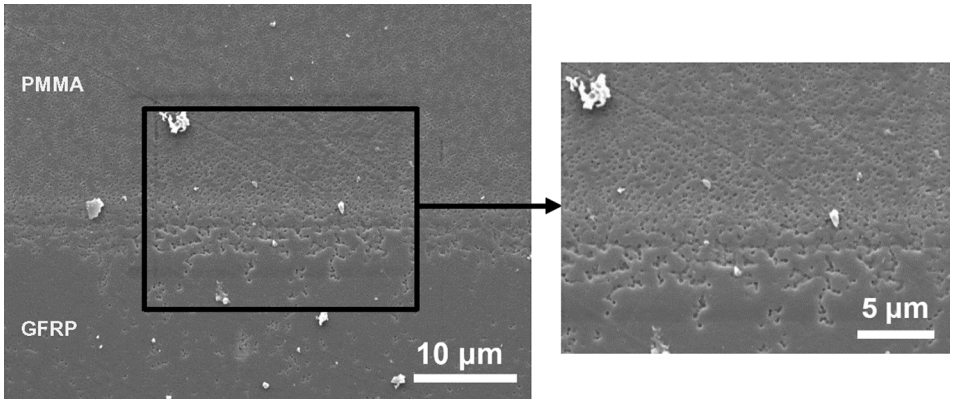

Fig. 6. Cross-sectional SEM images of the PMMA/GFRP composite plate.

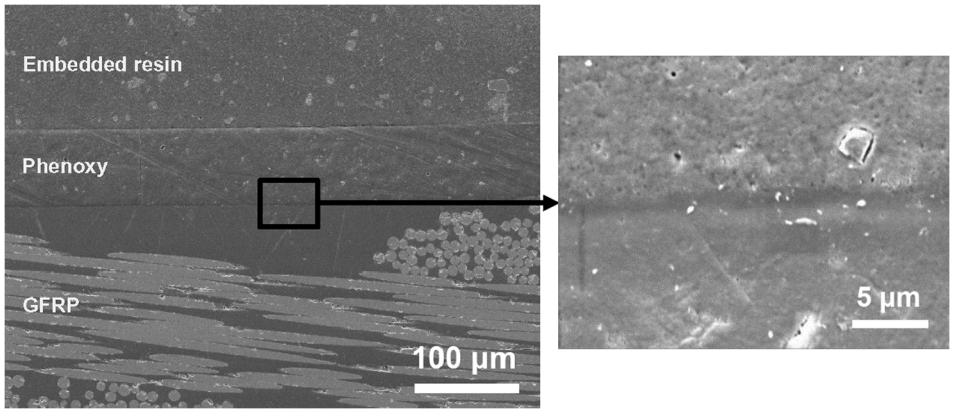

Fig. 7. Cross-sectional SEM images of the phenoxy/GFRP composite plate prepared with MVI.

Table 3
Experimentally determined Raman single spectrum parameters.

Parameter	Value (PMMA/GFRP)	Value (phenoxy/GFRP)
Laser	532 nm	638 nm
Power	10 mW	3 mW
Lens	×100	×100
Accumulations	2	2
Grafting	600 (750 nm)	600 (750 nm)
Acq. time	2 s	3 s

performed for both the PMMA/GFRP and phenoxy/GFRP samples, where multiple spectra were recorded across a defined thickness. This method, which is used to visualise and quantify molecular changes from one material to another, is based on the fact that the Raman peak intensity decreases as soon as the interphase begins and further decreases until none of the first material remains. Fig. 9 presents the relative concentrations for both combinations, illustrating the visible concentration gradients.

PMMA/GFRP: Each spectrum was recorded with the parameters in Table 3. A relatively low laser power of 10 mW was used due to the sensitivity of the polymers to the lasers. Here, relative Raman shifts of 1733 cm^{-1} for PMMA and 3071 cm^{-1} for epoxy were used to identify the

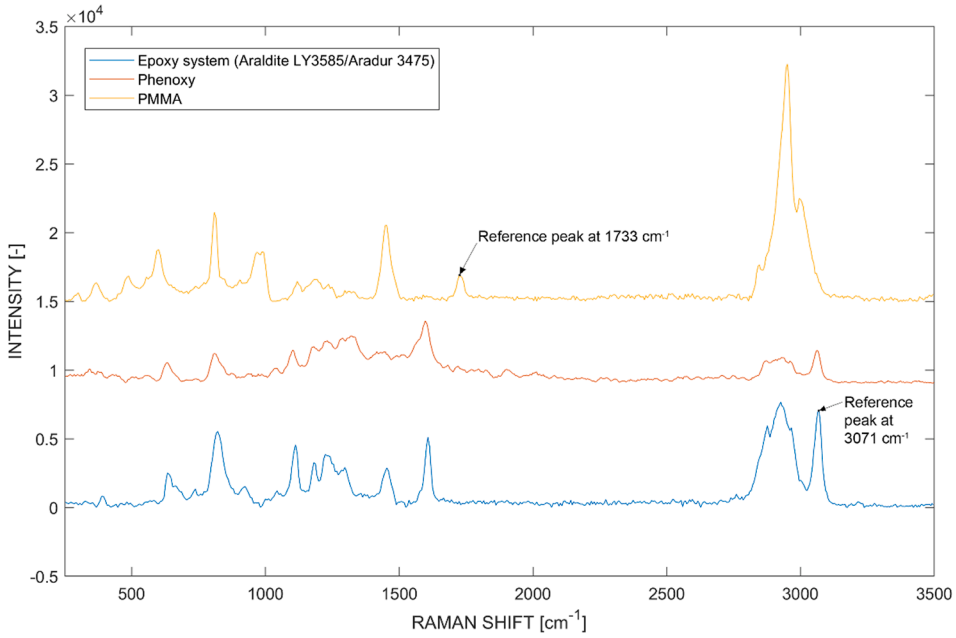

Fig. 8. Raman spectra of PMMA, phenoxy, and the cured epoxy system (Araldite LY3585/Aradur 3475). (For interpretation of the references to colour in this figure legend, the reader is referred to the web version of this article.)

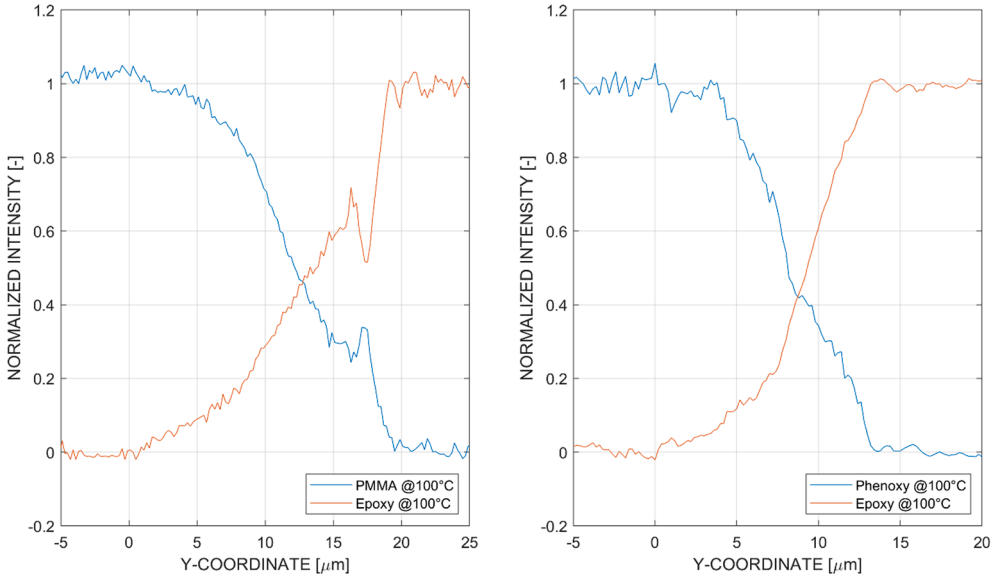

Fig. 9. Left: Relative PMMA and epoxy concentrations across the interphase for a sample subjected to a curing temperature of 100 °C based on the Raman peak intensities at 1733 cm^{-1} (PMMA) and 3071 cm^{-1} (epoxy). Right: Relative phenoxy and epoxy concentrations across the interphase for a sample subjected to a curing temperature of 100 °C based on classical least-squares fitting of both signals to pure reference spectra. (For interpretation of the references to colour in this figure legend, the reader is referred to the web version of this article.)

gradient interphase and are marked in black in Fig. 8. As shown in Fig. 9, a non-linear gradient was observed in the interphase of PMMA and the epoxy system. This measurement allowed for quantification of the interphase thickness during the curing reaction. Isothermal curing conditions at 100 °C resulted in a developed interphase with a thickness of 19 μm. Further investigation should focus on the curing temperature dependency of this phenomena. If the curing temperature were increased, a greater diffusion length would be unlikely because the reaction would occur much faster.

Phenoxy/GFRP: No characteristic peaks were identified by comparison of the spectra. Therefore, the pure signals for each constituent from the spectra measured across the interphase were fitted by classical least squares analysis. As a result, it was possible to quantify the interphase of the phenoxy/GFRP sample. A gradient interphase based on pure reaction–diffusion without the onset of phase separation was observed. For isothermal curing conditions at 100 °C, the thickness of the developed interphase was 13 μm.

3.3. Resistance welding and evaluation of mechanical performance

Several welding experiments were conducted for each thermoplastic material including PA12TR90/GFRP samples that did not display a satisfactory connection to the composite plate. The process parameters were approximated for all thermoplastics by directly correlating the total energy to the glass transition temperature, which allows for an estimation of the time when the polymer begins to flow during the welding process. This is further explained by Fig. 10, which gives an overview of the welding process with the determined parameters. The pressure increases as soon as power is introduced into the welding area due to compaction. The pressure reaches a maximum (see annotation 1) and then decreases because the amorphous thermoplastic reaches a high temperature and thus above glass transition temperature has a

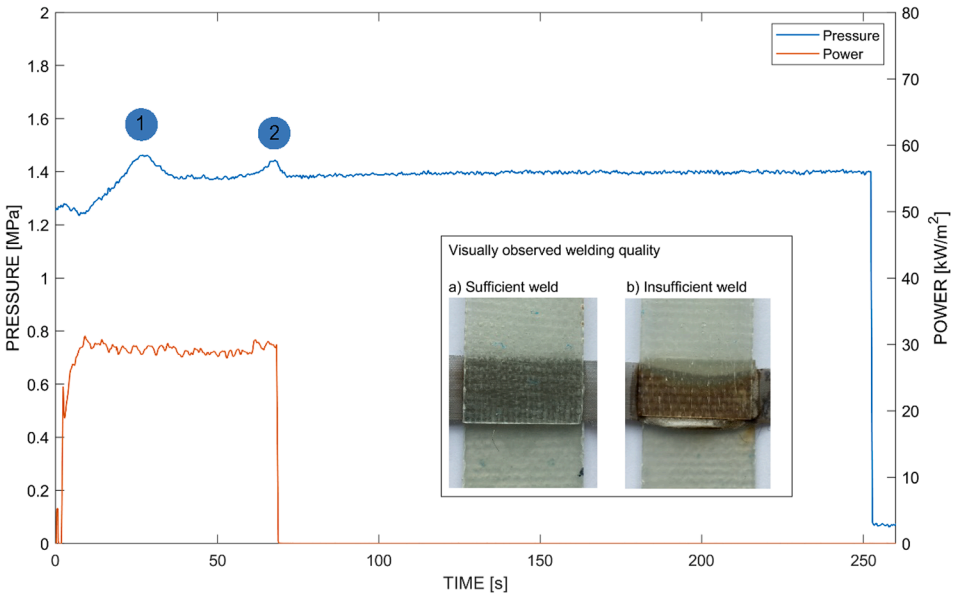

Fig. 10. In-situ power, pressure, and time measurements of lap shear coupon sample with a PMMA/GFRP configuration and additional images showing the visually observed welding quality. (For interpretation of the references to colour in this figure legend, the reader is referred to the web version of this article.)

sufficiently low viscosity to impregnate the steel mesh. Within this consolidation step, trapped air in the steel mesh can be avoided. The next region is characterised by thermal expansion arising from the fixed contact and further increase in temperature. At the maximum pressure (see annotation 2), the thermoplastic has reached its processing temperature, which leads to melt flow and a pressure loss from quench flow in the welded joint. In the fifth step, the voltage is switched off and cooling begins. The molten material continues to flow until the temperature is below the glass transition temperature. Therefore, pressure is applied to the welded area for another 180 s [25]. Ten welded samples were necessary to determine the favourable processing parameters for PMMA/GFRP as 30 kW/m^2, 60 s, and 1.2 MPa. Shown on the left is a sufficient weld with a well-consolidated steel mesh. In addition, the pressure–temperature coupling was well balanced to prevent quench flow of the thermoplastic out of the welding area. This can be considered as well-developed welding quality. In contrast, shown on the right is an example of insufficient welding due to high energy. In this case, the epoxy began to degrade, as indicated by the change in colour to brown. Furthermore, the temperature–pressure coupling was too high, and thus the steel mesh shifted within the welding area due to quench flow and the resulting high shear forces.

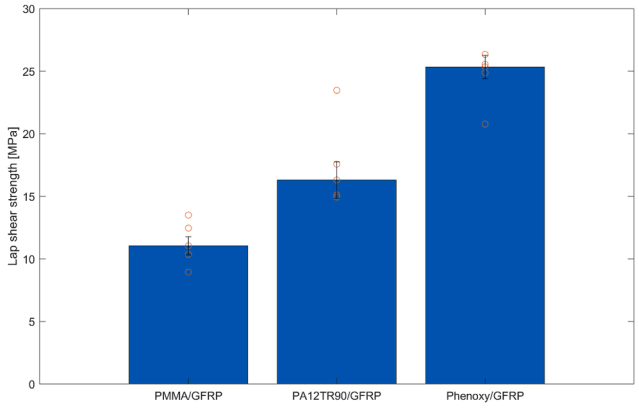

Fig. 11. Median, standard deviation, and scattered results of the tested lap shear coupons of PMMA/GFRP, PA12TR90/GFRP, and phenoxy/GFRP. (For interpretation of the references to colour in this figure legend, the reader is referred to the web version of this article.)

Fig. 11 illustrates the connection strength between two welded GFRP coupons with their respective thermoplastic boundary layers. The optimal processing parameters were empirically determined by systematic variation of the welding for each thermoplastic material. The determined process parameters were as follows, noted according to power/time/pressure: PMMA (25/40/1.6), PA12TR90 (30/60/1.2), and phenoxy (25/50/1.2). To obtain a representative strength, five welding trials were performed with the same processing parameters, and average values and standard deviations were calculated.

Additionally, the fracture behaviours were investigated by mechanical testing to ensure a complete analysis of the welding behaviour (Fig. 12). PMMA/GFRP presented an excellent welding quality with a well-impregnated steel mesh with an average lap shear strength of 11 MPa and standard deviation of 1.45 MPa. However, the coupons failed by adhesive failure between the epoxy and thermoplastic boundary layer, indicating that the full-strength potential was reached. Even increasing the welding thickness by adding additional layers to reduce the excessive shear stress did not increase or decrease the lap shear strength. It was reported by Ranganathaiah [23] that free volume holes can form between PMMA and epoxy due to debonding of the dispersed phase (PMMA) from the continuous phase (epoxy). This was also observed by the Raman line scans (Fig. 9), where a relative concentration drop was apparent at 18 μm. This decrease corresponds to the onset of phase separation as previously identified by Teuwen *et al.* [3]. The observed concentration decrease in the PMMA/GFRP samples is distinctive with respect to the concentration gradient and can lead to weakening of the interphase strength, which can cause adhesive failure.

PA12TR90/GFRP was also analysed in the welding study although no interphase formed between the epoxy and boundary layer. Despite this fact, the welding proved to be reliable with an average lap shear strength of 16.3 MPa and standard deviation of 2.9 MPa. In most cases, the thermoplastic boundary layer fell off after the composite plate was demoulded. For the welding trials, the films which fell off were laid between the welding stack and then heated. These adhesion phenomena provide a potential hypothesis for the good welding performance: mechanical coupling and/or molecular bonding. In summary, mechanical coupling arises from the well-impregnated porous surface of the adhesive, which in our case is PA12TR90. In addition, molecular bonding can occur as a result of intermolecular forces between the adhesive and substrate such as dipole–dipole interactions, van der Waals forces, and

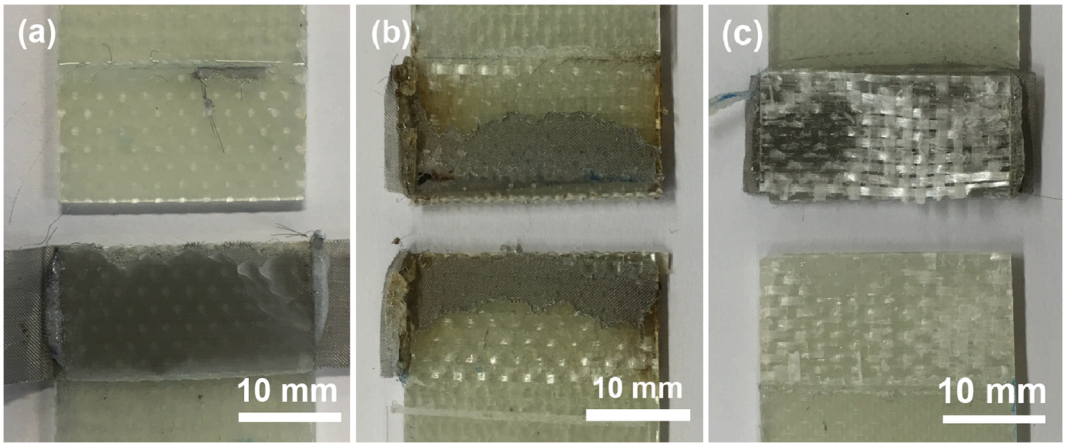

Fig. 12. Fracture analysis of tested lap shear coupons. (a) PMMA/GFRP: Adhesive failure between interphase. (b) PA12TR90/GFRP: Mainly cohesive failure. (c) Phenoxy/GFRP: Dominant composite failure. (For interpretation of the references to colour in this figure legend, the reader is referred to the web version of this article.)

chemical interactions. This mechanism describes the strength of the adhesive joints according to the interfacial forces and the presence of polar groups [7].

Phenoxy/GFRP was the most promising material in this study with an average lap shear strength of 25.3 MPa and standard deviation of 1.85 MPa. This is because of the high diffusion between the epoxy system and boundary layer, as well as the favourable adhesion and mechanical strength of the characterised lap shear coupons. The fracture mode shown in Fig. 12 is dominantly composite failure, where at first the glass fibre ply had broken out. This was a strong indication that the interphase between phenoxy and the epoxy was stronger than the constituents, illustrating the potential of a quickly developed intersection between the thermoplastic and epoxy. As stated before, phenoxy is based on bisphenol A and epichlorohydrin, which is the same base material as the epoxy precursor Araldite LY3585.

4. Conclusion

This study presents a procedure for characterising the interphase evolution between a thermoplastic and thermoset polymer with methodologies including optical hot-stage microscopy and mechanical testing of welded lap shear coupons. PMMA, PA12TR90, and phenoxy were chosen as suitable thermoplastic polymers. Additionally, a fast-curing epoxy system (Araldite LY3585/Aradur 3475) suitable for automotive applications was chosen for this study, which made it difficult to observe pronounced dissolution and diffusion processes due to their dependence on time and temperature. In-depth analysis with the hot-stage experiments as well as the Raman spectroscopy enabled a strong understanding of the influence of material properties, solubility, and diffusion on the formation mechanisms. PMMA and phenoxy presented the highest affinity towards the epoxy system due to their high chain mobility, fast dissolution, and high diffusion rate, where the materials exhibited simultaneous diffusion with the epoxy system. An interphase thickness of 19 μm for PMMA and 13 μm for phenoxy was measured by Raman spectroscopy for a curing temperature of 100 °C, where phase separation occurred with PMMA throughout the interphase area. In contrast, phenoxy did not result in visible phase separation. PA12TR90 did not show a pronounced interaction with the epoxy system.

Furthermore, to evaluate the mechanical strength, several glass-fibre-reinforced polymer plates were manufactured with the innovative coupling of MVI and co-curing of the thermoplastic boundary layer. PMMA, PA12TR90, and phenoxy were used for first trials with a resistance welding setup to weld lap shear coupons and determine their mechanical properties with a tensile test machine. Phenoxy had an average lap shear strength of 26 MPa and exhibited cohesive failure in the composite, indicating the strong and reliable potential of the joints. PA12TR90 also presented high values despite the fact that no interphase formed. Thus, both thermoplastic polymers exhibit adhesion mechanisms based on molecular chain bridging and mechanical coupling.

Within this study, it was possible to push the limits of using a thermoplastic as a boundary layer for a fast-curing epoxy system for automotive applications with a final glass transition temperature of approximately 120 °C. The manufactured composite plates were used for a resistance welding application, which enabled strong connections in less than 4 min. This shows the potential of using a thermoplastic boundary layer for welding purposes with respect to industrial application in the fields of transportation and wind energy. Future work will focus on implementation into an actual component and thereby derive the sensitivities and limits of the presented joining technology.

Funding

The authors disclose receipt of the following financial support for the research, authorship and/or publication of this article: This study was supported by the national funded project Cafimp [grant number 25320], which was supported by Innosuisse, Switzerland.

CRediT authorship contribution statement

Lucian Zweifel: Methodology, Software, Investigation, Writing - original draft, Writing - review & editing, Visualization. **Christian Brauner:** Conceptualization, Supervision, Project administration.

Declaration of Competing Interest

The authors declare no potential conflicts of interest with respect to the research, authorship, and/or publication of this article.

Acknowledgements

The authors would like to thank Gabriel Chem. that was represented by Michel Lenoble for supplying materials, and Clemens Dransfeld, Professor of Aerospace Manufacturing Technologies at TU Delft for the support in the project.

References

[1] Schürmann H. Konstruieren mit Faser-Kunststoff- Verbunden. Springer Berlin; 2007. https://doi.org/10.1007/b137636.
[2] Brauner C, Nakouzi S, Zweifel L, Tresch J. Co-curing behaviour of thermoset composites with a thermoplastic boundary layer for welding purposes. Advanced Composites Letters 2020;29:1–9. https://doi.org/10.1177/2633366X20902777.

[3] Teuwen JJE, Asquier J, Inderkum P, Masania K, Brauner C, Villegas IF, et al. Gradient interphases between high Tg epoxy and polyetherimide for advanced joining processes. In: Proceedings of ECCM-18 Conference. Athens, June, 2018.
[4] Villegas IF, van Moorleghem R. Ultrasonic welding of carbon/epoxy and carbon/PEEK composites through a PEI thermoplastic coupling layer. Compos A Appl Sci Manuf 2018;109:75–83.
[5] Ageorges C, Ye L, Hou M. Advances in fusion bonding techniques for joining thermoplastic matrix composites: a review. Compos A Appl Sci Manuf 2001;32(6):839–57.
[6] Shi H. Resistance welding of thermoplastic composites. TU Delft 2014.
[7] Zweifel L, Brunner J, Brauner C, Dransfeld C. Development of a resistance welding process for thermoset fiber composite components with co-cured thermoplastic boundary layer. In: Proceedings of ECCM-18 Conference. Athens, June, 2018.
[8] Palardy G, Villegas IF. Smart ultrasonic welding of thermoplastic composites. Proc. Am. Soc. Compos. - 31st Tech. Conf. ASC 2016.
[9] van Krevelen DWW. Properties of Polymers. Elsevier 2009. https://doi.org/10.1016/B978-0-444-82877-4.50021-4.
[10] Lestriez B, Chapel J-P, Gérard J-F. Gradient Interphase between Reactive Epoxy and Glassy Thermoplastic from Dissolution Process, Reaction Kinetics, and Phase Separation Thermodynamics. Macromolecules 2001;34(5):1204–13.
[11] Park JW, Kim S.C. Processing of Composites. In: Davé R, Loos A, editors., Carl Hanser Verlag; 1999.
[12] Shi H, Villegas IF, Octeau M-A, Bersee HEN, Yousefpour A. Continuous resistance welding of thermoplastic composites: Modelling of heat generation and heat transfer. Compos A Appl Sci Manuf 2015;70:16–26.
[13] Tsiangou E, Teixeira de Freitas S, Fernandez Villegas I, Benedictus R. Investigation on energy director-less ultrasonic welding of polyetherimide (PEI)- to epoxy-based composites. Compos B Eng 2019;173:107014. https://doi.org/10.1016/j.compositesb:2019.107014.
[14] Solvay. FM® 309-1 film adhesive product datasheet. Alpharetta, USA; 2018.
[15] Sika Deutschland GmbH. SikaPower®-1200 product datasheet. Stuttgart, Germany; 2020.
[16] Manias E, Utracki LA. 4 . Thermodynamics of Polymer Blends 2014:25–9. https://doi.org/10.1007/978-94-007-6064-6.
[17] JEC. Huntsman Advanced Materials optimises auto composites series applications 2014. (accessed June 19, 2020). http://www.jeccomposites.com/knowledge/international-composites-news/huntsman-advanced-materials-optimises-auto-composites-series.
[18] Garschke C, Parlevliet PP, Weimer C, Fox BL. Cure kinetics and viscosity modelling of a high-performance epoxy resin film. Polym Test 2013;32(1):150–7.
[19] Chem Gabriel. Gabriel Phenoxy PK™FE natural film product datasheet. USA: Akron (OH); 2018.
[20] EMS Chemie AG. Polyamid Grilamid TR 90 product datasheet. Domat/Ems, Switzerland; 2017.
[21] Evonik Röhm GmbH. PMMA No. 99524 natural film product datasheet. Darmstadt, Germany; 2011.
[22] Shi H, Villegas IF, Bersee HEN. Strength and failure modes in resistance welded thermoplastic composite joints: Effect of fibre–matrix adhesion and fibre orientation. Compos A Appl Sci Manuf 2013;55:1–10.
[23] Dubé M, Hubert P, Gallet JNAH, Stavrov D, Bersee HEN, Yousefpour A. Metal mesh heating element size effect in resistance welding of thermoplastic composites. J Compos Mater 2012;46(8):911–9.
[24] Van Velthem P, Ballout W, Daoust D, Sclavons M, Cordenier F, Henry E, Dumont D, Destoop V, Pardoen T, Bailly C. Influence of thermoplastic diffusion on morphology gradient and on delamination toughness of RTM-manufactured composites. Compos A Appl Sci Manuf 2015;72:175–83.
[25] Stavrov D, Bersee HEN. Resistance welding of thermoplastic composites-an overview. Compos A Appl Sci Manuf 2005;36(1):39–54.
[26] Ravikumar HB, Ranganathaiah C, Kumaraswamy GN, Siddaramaiah. Influence of free volume on the mechanical properties of Epoxy/poly (methylmethacrylate) blends. J Mater Sci 2005;40(24):6523–7.
[27] Rastegar Saeed, Mohammadi Naser, Bagheri Reza. Development of co-continuous morphology in epoxy poly(methyl methacrylate) (PMMA) blends cured by mixtures of phase-separating and non-phase-separating curing agents. Colloid Polym Sci 2004;283(2):145–53.